

Visualization of a short-range Wnt gradient in the intestinal stem-cell niche

Henner F. Farin^{1,2,3,4}, Ingrid Jordens⁵, Mohammed H. Mosa^{2,3,4}, Onur Basak¹, Jeroen Korving¹, Daniele V. F. Tauriello⁵, Karin de Punder⁶, Stephane Angers⁷, Peter J. Peters⁶, Madelon M. Maurice^{5*} & Hans Clevers^{1*}

Mammalian Wnt proteins are believed to act as short-range signals^{1–4}, yet have not been previously visualized *in vivo*. Self-renewal, proliferation and differentiation are coordinated along a putative Wnt gradient in the intestinal crypt⁵. Wnt3 is produced specifically by Paneth cells^{6,7}. Here we have generated an epitope-tagged, functional Wnt3 knock-in allele. Wnt3 covers basolateral membranes of neighbouring stem cells. In intestinal organoids, Wnt3-transfer involves direct contact between Paneth cells and stem cells. Plasma membrane localization requires surface expression of Frizzled receptors, which in turn is regulated by the transmembrane E3 ligases Rnf43/Znrf3 and their antagonists Lgr4-5/R-spondin. By manipulating Wnt3 secretion and by arresting stem-cell proliferation, we demonstrate that Wnt3 mainly travels away from its source in a cell-bound manner through cell division, and not through diffusion. We conclude that stem-cell membranes constitute a reservoir for Wnt proteins, while Frizzled receptor turnover and ‘plasma membrane dilution’ through cell division shape the epithelial Wnt3 gradient.

Distinct mechanisms have been proposed as to how gradients of secreted Wnt protein control growth and patterning during animal development. Evidence exists for highly localized activity between adjacent cells^{1–3}, as well as for long-range activity^{8,9}. *Drosophila* Wingless (Wg) is classically considered a morphogen in the wing imaginal disk, secreted from a stripe of cells to form a long-range concentration gradient^{10–12}. This concept was recently challenged, when it was shown that membrane tethering of Wg to the producer cells did not perturb early development⁴. In vertebrates, limited information exists on endogenous Wnt protein distribution¹³, and on how Wnt gradients are built and maintained. Transcriptional Wnt target gene activity has been well-characterized in the Wnt-dependent stem-cell compartment of intestinal crypts⁵. Expression of Wnt target genes occurs in a gradient¹⁴, with highest activity at the crypt bottom where Lgr5⁺ stem cells¹⁵ are located between post-mitotic Paneth cells, that produce high levels of Wnt3 (refs 6, 7). Paneth-cell-derived Wnt3 is redundant with mesenchymally produced Wnts *in vivo*^{16,17}. In three-dimensional organoid culture, Lgr5 stem cells generate ever-growing, self-organizing ‘mini-guts’ with defined crypt- and villus-domains¹⁸, a process for which Paneth-cell-derived Wnt3 is essential¹⁶. In the current study, we exploit the mammalian mini-gut system as an experimental equivalent of the fly imaginal disk to dissect paracrine Wnt signalling.

We generated a mouse *Wnt3* allele, by introducing an haemagglutinin (HA)-tag at position Q41, located in a weakly conserved surface region opposite the Frizzled receptor binding site¹⁹ (Fig. 1a and Extended Data Fig. 1). This tagging strategy is more generally applicable to different Wnt members and peptide epitopes (Extended Data Fig. 2). While homozygous loss of *Wnt3* in mice causes gastrulation

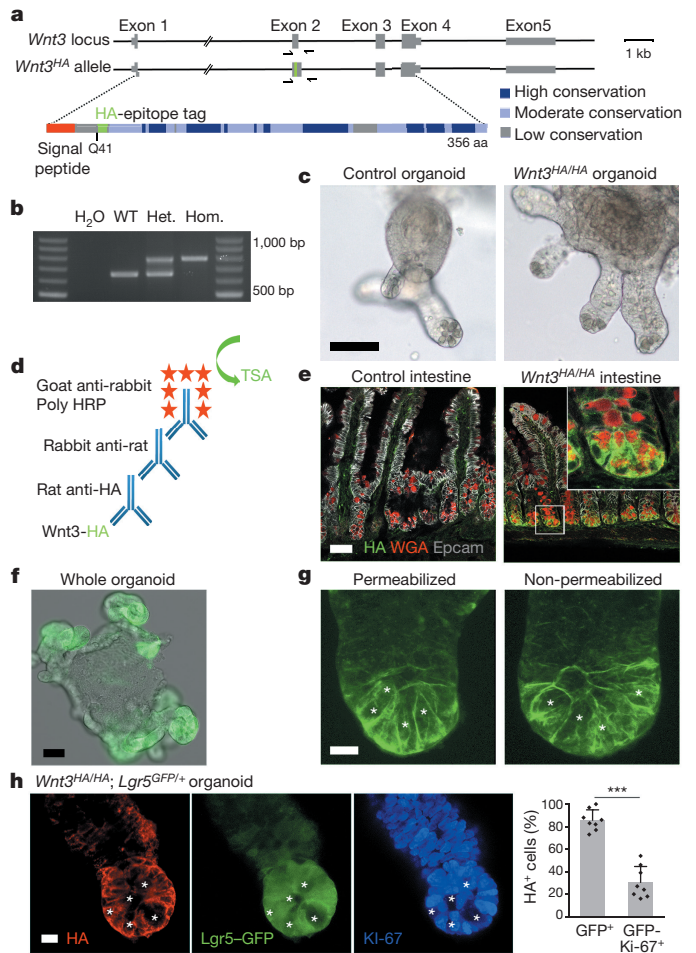


Figure 1 | Endogenous Wnt3 protein is localized to basolateral plasma membranes in the intestinal crypt. **a**, Generation of a Wnt3-HA knock-in allele. **b**, PCR genotyping; *Wnt3*^{HA/HA} mice are viable. WT, wild type. **c**, Morphology of organoid cultures. **d**, HA immunodetection protocol using tyramide signal amplification (TSA). **e**, Confocal imaging in intestinal tissues. Co-staining of HA, Epcam (membranes) and WGA (secretory granules). **f**, Whole-mount staining of *Wnt3*^{HA/HA} organoid. **g**, Wnt3 signal on crypt membranes is independent of permeabilization. Three-dimensional projected confocal images (see Supplementary Video 2). **h**, Staining in *Wnt3*^{HA/HA}; *Lgr5*^{EGFP/+} organoids. Enriched signal on stem cells (*Lgr5*-GFP⁺) compared with TA cells (Ki-67⁺/*Lgr5*-GFP⁻). Quantification in *n* = 8 organoids (mean ± s.d.; *P* < 10⁻⁶; *t*-test). Scale bars, 50 μm (**c**, **e**, **f**) and 10 μm (**g**, **h**). Paneth cells were identified on the basis of morphology and labelled by asterisks.

¹Hubrecht Institute, Royal Netherlands Academy of Arts and Sciences (KNAW) and University Medical Center Utrecht, 3584CT Utrecht, the Netherlands. ²German Cancer Consortium (DKTK), 69120 Heidelberg, Germany. ³Georg-Speyer-Haus, Institute for Tumor Biology and Experimental Therapy, 60596 Frankfurt am Main, Germany. ⁴German Cancer Research Center (DKFZ), 69120 Heidelberg, Germany. ⁵Department of Cell Biology, Center for Molecular Medicine, University Medical Center Utrecht, 3584CX Utrecht, the Netherlands. ⁶The Maastricht Multimodal Molecular Imaging institute, Maastricht University, 6229ER Maastricht, the Netherlands. ⁷Leslie Dan Faculty of Pharmacy, University of Toronto, Toronto, Ontario M5S 3M2, Canada.

*These authors contributed equally to this work.

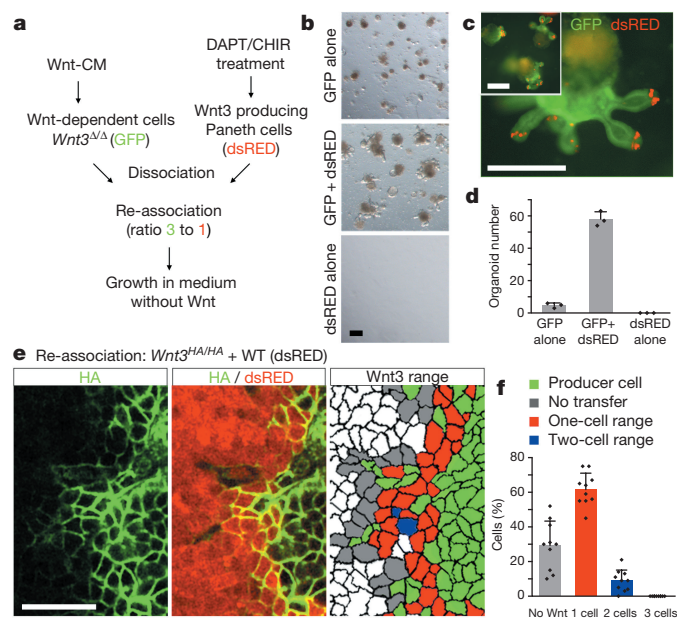


Figure 2 | Wnt3 transfer requires direct cell contact and has a limited range. **a–d**, Cell re-association of Wnt-dependent ($Wnt3^{\Delta/\Delta}$) with Wnt3-producing Paneth cells. **a**, Experimental protocol; **b**, light microscopic; and **c**, epifluorescent images. Self-organization of crypts with dsRED-expressing Paneth cells. **d**, Mean organoid number (\pm s.d.) in $n = 3$ independent wells after 10 days. **e**, Measurement of epithelial Wnt3-range. Re-association using Wnt3-HA producing cells (non-labelled) and wild-type cells expressing dsRED. Z-projected confocal images and colour-coding depending on the distance to the closest Wnt3-HA producing cell. **f**, Average percentage (\pm s.d.) of each distance fraction in $n = 10$ organoids. Scale bars, 200 μ m (**b**, **c**) and 25 μ m (**e**).

arrest²⁰, $Wnt3^{HA/HA}$ knock-in mice are viable and fertile (Fig. 1b). To study pathway activity, we collected crypts from homozygous and control mice either directly, or after 2 weeks of mini-gut culture. Quantitative reverse transcription PCR (RT-qPCR) analysis showed no differences in the levels of Wnt target gene expression (Extended Data Fig. 3). In concordance, $Wnt3^{HA/HA}$ organoids displayed normal growth and morphology (Fig. 1c). Together, the internal HA-tag fully preserved Wnt3 function.

Western blot analysis of mini-guts revealed low expression of the Wnt3-HA protein, only detectable after conversion of all cells into Wnt3-producing Paneth cells²¹ (Extended Data Fig. 4a, b). On intestinal sections, a multi-step amplification protocol allowed specific Wnt3-HA detection in Paneth cells (Fig. 1d, e). Paneth cell granules were negative, implying that Wnt3 is not secreted via this dominant, apical secretion route (Extended Data Fig. 4c, d and Supplementary Video 1). To obtain high-resolution information in a system amenable to experimental manipulation, we derived mini-guts from homozygous knock-in mice. We observed fluorescence exclusively in the crypt equivalents within the mini-guts, while the villus-domain was negative (Fig. 1f). Confocal laser microscopy demonstrated that Wnt3 covers basolateral crypt membranes (Fig. 1g, Extended Data Fig. 4e, f and Supplementary Video 2). This staining pattern was not dependent on membrane permeabilization, indicating that Wnt3 is mainly localized on the external cell surface. Co-localization with the $Lgr5^{EGFP}$ reporter¹⁵ and KI-67 showed a specific enrichment on $Lgr5$ stem cells compared with transit-amplifying (TA) cells (Fig. 1h).

To determine whether the mini-gut cultures secrete diffusible Wnt activity, we tested if Wnt3-producing, wild-type organoids could rescue the growth of $Wnt3^{\Delta/\Delta}$ (knockout) cultures. Fluorescently labelled mini-guts were co-seeded in Matrigel. We found that the presence of wild type (dsRED) did not support growth of $Wnt3^{\Delta/\Delta}$ mini-guts (green fluorescent protein, GFP) (Extended Data Fig. 5a–d), arguing that diffusible Wnt activity was negligible. Consistently, we could

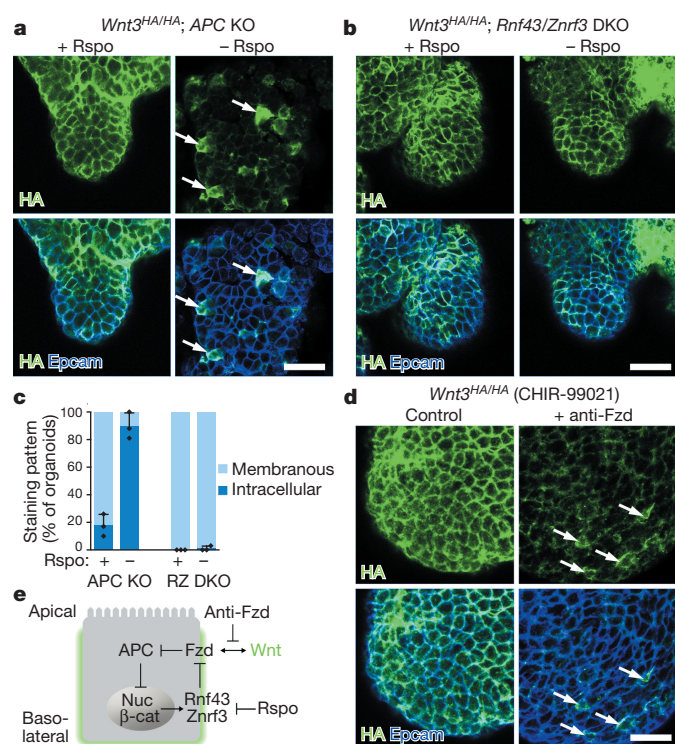


Figure 3 | Frizzled receptors act as membrane tether of Wnt3.

a, **b**, R-spondin (Rspo) controls membrane localization in APC knockout (**a**) but not in $Rnf43/Znrf3$ double mutants (RZ DKO; **b**). Epcam staining of cell membranes; arrows show intracellular staining. **c**, Mean percentage of organoids (\pm s.d.) with membranous or intracellular staining. Data from $n = 3$ independent experiments. **d**, Neutralizing pan-Frizzled antibody (anti-Fzd) reduces surface expression of Wnt3-HA with residual intracellular signal (arrows). Treatment for 48 h; CHIR-99021 was added to rescue organoid growth. The z-projections of confocal images are shown; all scale bars, 25 μ m. **e**, Model for control of the Wnt3 localization by Frizzled and the E3 ligases $Rnf43/Znrf3$.

neither detect transfer of Wnt3-HA between organoids, nor interfere with growth of $Wnt3^{HA/HA}$ cultures by embedding anti-HA affinity beads that efficiently sequester diffusible factor (Extended Data Fig. 5e, f).

To investigate direct protein transfer between adjacent epithelial cells, we performed re-association assays after single-cell dispersal of fluorescently labelled organoids. GFP-expressing $Wnt3^{\Delta/\Delta}$ cells were mixed with *in vitro* differentiated wild-type Paneth cells (dsRED). Aggregates were transferred to Matrigel and cultured in the absence of exogenous Wnt (see experimental scheme in Fig. 2a). Wild-type Paneth cells rescued the growth of $Wnt3^{\Delta/\Delta}$ cells (Fig. 2b–d). We observed efficient self-organization into crypt structures with a stereotypic arrangement of dsRED-labelled cells at the budding tips (Fig. 2c), consistent with the model that Paneth cells serve as symmetry-breaking crypt organizers in culture. Staining revealed spatial confinement of Wnt3-HA around individual Paneth cells (Supplementary Video 3). To measure the extent of Wnt3 propagation within the epithelial sheet more easily, we generated spherical organoids (by addition of Wnt3a-conditioned medium (CM))⁷. Interfaces between Wnt3-HA-producing cells (non-labelled) and wild-type receiving cells (dsRED-labelled, which only express non-tagged Wnt) were readily recognizable. Wnt3-HA penetrated one cell diameter (two at the most) into the Wnt3-HA-negative domains (Fig. 2e, f). Strong differences in Wnt3-HA decoration were observed between adjacent cells. Thus, localized production and limited epithelial spreading appeared important hallmarks of Wnt3 distribution.

We subsequently investigated if Wnt3-HA binding to stem-cell membranes depends on its cognate Frizzled receptors. As crypts

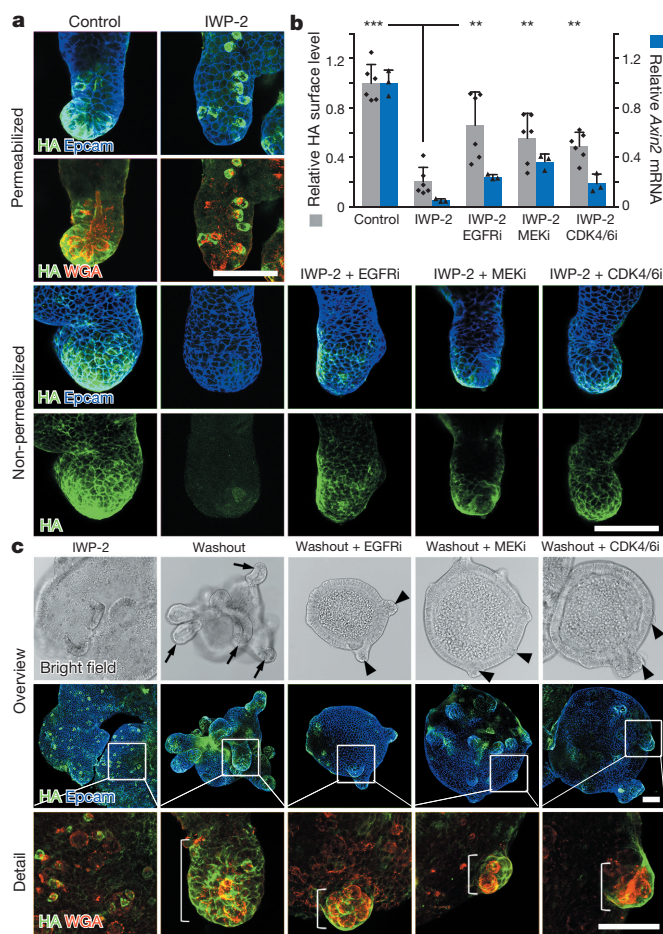


Figure 4 | Cell proliferation influences Wnt3 surface level and signal range. **a**, Chase experiment: 24 h after block of Wnt-production (IWP-2), Wnt3-HA is sequestered in WGA-positive Paneth cells (top) and absent from the cell surface (non-permeabilized samples; bottom). Parallel block of proliferation by inhibitors of EGFR, MEK or CDK4/6 causes retention of surface HA signal. **b**, Quantification of Wnt3 surface level and transcriptional activity. Grey bars, mean HA-staining intensity in $n = 6$ non-permeabilized organoids per condition. Blue bars, mean *Axin2* expression in $n = 3$ independent wells; error bars, s.d.; *t*-test compared with IWP-2 condition: *** $P < 10^{-3}$, ** $P < 10^{-2}$. **c**, Pulse experiment after Wnt-release (washout of IWP-2/Wnt-CM). Crypts formed in normal medium (arrows) are positive for Wnt3-HA. After block of proliferation, rudimentary crypts are formed (arrowheads) and the Wnt3-HA signal remains focused (brackets). Z-projected confocal images. All scale bars, 50 μm .

express multiple Frizzleds⁶, we altered their surface expression indirectly by modulation of the transmembrane E3-ligases Rnf43 and Znr3. These act as negative feedback regulators of Wnt signaling by ubiquitinylation and subsequent lysosomal degradation of Frizzleds^{22,23}. Of note, Lgr4/5 proteins and their R-spondin ligands antagonize Frizzled downregulation by recruiting Rnf43/Znr3 into a trimeric complex^{22,24}. Given that organoid growth requires R-spondin¹⁸, we first tested its effect on Wnt localization. We found that the Wnt3-HA signal expanded or decreased in an R-spondin1 concentration-dependent manner (Extended Data Fig. 6a). Because *Wnt3* transcription was also strongly R-spondin-dependent (Extended Data Fig. 6b), we aimed to uncouple the effect of R-spondin on Frizzled-turnover from downstream signalling. To this end, we genetically activated the pathway in *Wnt3^{HA/HA}* cultures. CRISPR/Cas9-induced null mutations in *APC* or in *Rnf43/Znr3* (Extended Data Fig. 7)²⁵ resulted in R-spondin-independent growth. Wnt3-HA was absent from the surface of *APC* mutant mini-guts (that express high levels of Rnf43/Znr3), but could be restored by addition of

R-spondin (Fig. 3a, c). This implied that Frizzleds tether Wnt3 to membranes, as has been suggested in the *Drosophila* wing disc²⁶. Consistently, Wnt3 surface localization was high and insensitive to R-spondin in *Rnf43/Znr3* mutant cultures (Fig. 3b, c). In cell re-association assays, Wnt3-HA transfer to *Rnf43/Znr3* mutant cells was increased and to *APC* mutant cells was reduced (Extended Data Fig. 8). Independently, the application of a neutralizing pan-Frizzled antibody²⁷ strongly reduced Wnt3-HA surface expression (Fig. 3d). Together, these experiments indicate that surface-expressed Frizzled binds and retains Wnt3 (Fig. 3e).

To explore the kinetics of Wnt3 surface expression, we acutely blocked Wnt secretion using the Porcupine inhibitor IWP-2 (ref. 28). After 24 h, Wnt3-HA was observed exclusively inside Paneth cells, highlighting the requirement of Porcupine for Wnt trafficking to the plasma membrane of these cells (Fig. 4a). Staining of non-permeabilized organoids confirmed that surface-bound Wnt3 was absent, indicating that its half-life is below 24 h. To test if cell division has an impact on propagation of surface-bound Wnt3, we induced cell cycle arrest using the EGF-receptor inhibitor Gefitinib, the downstream MEK inhibitor PD-0325901, or the CDK4/6 inhibitor Palbociclib (Extended Data Fig. 9a, b). In all cases, residual Wnt3 surface signal and increased transcriptional activity was observed 24 h after initiation of IWP-2 treatment (Fig. 4a, b), indicating that cell division under normal conditions dilutes cell-bound Wnt3.

To address if cell division is indeed the means by which Wnt3 is propagated from the Paneth cell source, we blocked Wnt secretion for 3 days, followed by washout of the Porcupine inhibitor. Formation of multiple crypt-like structures, invariably decorated with a gradient of Wnt3-HA, was observed within 2 days after IWP-2 washout (Fig. 4c and Supplementary Video 4). In the presence of EGFR, MEK or CDK4/6 inhibitors, crypt formation was blocked and Wnt3-HA remained localized around the producing cells. These results suggest that signal propagation is dependent on cell division.

From these combined observations, we concluded that two phenomena control the size and shape of the short-range, graded Wnt3 signal. First, Wnt3, produced by Paneth cells, does not freely diffuse, but is transferred to the nearest neighbour, typically an *Lgr5* stem cell. Frizzled receptors tether Wnt to the membrane of the receiving stem cell. Surface expression of the Wnt-Frizzled complex is negatively controlled by Rnf43/Znr3, which in turn can be alleviated by Lgr4/5 and R-spondin. Second, Frizzled-bound Wnt spreads passively by stem-cell division, which dilutes surface-bound Wnt and thus creates a gradient.

Similar highly localized Wnt signals have been described in invertebrate models¹⁻³. Long-range signalling is dispensable during fly embryogenesis, but transfer over longer distances becomes important during post-juvenile organ growth⁴. Apparently, the body dimensions then become too large to support Wnt-signalling only by auto/juxtacrine sources. From an evolutionary perspective it is interesting that the R-spondin/Lgr Wnt signal amplifier is a vertebrate-specific innovation, while Rnf43 is already present in *Caenorhabditis elegans*. Organ size in vertebrates may require amplified cellular output from stem-cell niche compartments. The R-spondin/Lgr signalling module appears designed to prolong/increase Wnt surface levels once cells have left contact to the niche to build a TA compartment. Unlike the *Drosophila* wing disc, where autocrine Wnt signalling appears to predominate⁴, Wnt signalling is non-cell-autonomous and relies on the presence of dedicated niche Paneth cells as well as non-epithelial sources^{16,17}. Transfer within the epithelium requires direct Paneth cell contact (this study), a notion that is in agreement with our previous observation that stem cells attempt to maximize their membrane contact to Paneth cells⁷. This also explains why a central position of *Lgr5* stem cells between Paneth cells supports stem-cell maintenance more efficiently than a peripheral position²⁹. It has been demonstrated that topical application of Wnt (immobilized on a bead) to one side of a stem cell results in an asymmetrical outcome of the subsequent stem-cell division³⁰. Crypt stem cells located at the niche boundary

experience a similarly sharp Wnt gradient, as only one side of a 'boundary stem cell' touches its Wnt source, the Paneth cell. Stem-cell plasma membranes thus carry positional information that could be involved in timing of differentiation. How Wnt3 is transferred between producing and receiving cells remains to be determined.

Online Content Methods, along with any additional Extended Data display items and Source Data, are available in the online version of the paper; references unique to these sections appear only in the online paper.

Received 1 October; accepted 18 December 2015.

Published online 10 February 2016.

- van den Heuvel, M., Nusse, R., Johnston, P. & Lawrence, P. A. Distribution of the wingless gene product in *Drosophila* embryos: a protein involved in cell-cell communication. *Cell* **59**, 739–749 (1989).
- Thorpe, C. J., Schlesinger, A., Carter, J. C. & Bowerman, B. Wnt signaling polarizes an early *C. elegans* blastomere to distinguish endoderm from mesoderm. *Cell* **90**, 695–705 (1997).
- Goldstein, B., Takeshita, H., Mizumoto, K. & Sawa, H. Wnt signals can function as positional cues in establishing cell polarity. *Dev. Cell* **10**, 391–396 (2006).
- Alexandre, C., Baena-Lopez, A. & Vincent, J.-P. Patterning and growth control by membrane-tethered Wingless. *Nature* **505**, 180–185 (2014).
- Clevers, H. The intestinal crypt, a prototype stem cell compartment. *Cell* **154**, 274–284 (2013).
- Gregorieff, A. *et al.* Expression pattern of Wnt signaling components in the adult intestine. *Gastroenterology* **129**, 626–638 (2005).
- Sato, T. *et al.* Paneth cells constitute the niche for Lgr5 stem cells in intestinal crypts. *Nature* **469**, 415–418 (2011).
- Coudreuse, D. Y. M., Roël, G., Betist, M. C., Destrée, O. & Korswagen, H. C. Wnt gradient formation requires retromer function in Wnt-producing cells. *Science* **312**, 921–924 (2006).
- Kiecker, C. & Niehrs, C. A morphogen gradient of Wnt/ β -catenin signalling regulates anteroposterior neural patterning in *Xenopus*. *Development* **128**, 4189–4201 (2001).
- Zecca, M., Basler, K. & Struhl, G. Direct and long-range action of a wingless morphogen gradient. *Cell* **87**, 833–844 (1996).
- Neumann, C. J. & Cohen, S. M. Long-range action of Wingless organizes the dorsal-ventral axis of the *Drosophila* wing. *Development* **124**, 871–880 (1997).
- Strigini, M. & Cohen, S. M. Wingless gradient formation in the *Drosophila* wing. *Curr. Biol.* **10**, 293–300 (2000).
- Galli, L. M., Barnes, T. L., Secrest, S. S., Kadowaki, T. & Burrus, L. W. Porcupine-mediated lipid-modification regulates the activity and distribution of Wnt proteins in the chick neural tube. *Development* **134**, 3339–3348 (2007).
- Muñoz, J. *et al.* The Lgr5 intestinal stem cell signature: robust expression of proposed quiescent '+4' cell markers. *EMBO J.* **31**, 3079–3091 (2012).
- Barker, N. *et al.* Identification of stem cells in small intestine and colon by marker gene Lgr5. *Nature* **449**, 1003–1007 (2007).
- Farin, H. F., Van Es, J. H. & Clevers, H. Redundant sources of Wnt regulate intestinal stem cells and promote formation of Paneth cells. *Gastroenterology* **143**, 1518–1529.e7 (2012).
- Kabiri, Z. *et al.* Stroma provides an intestinal stem cell niche in the absence of epithelial Wnts. *Development* **141**, 2206–2215 (2014).
- Sato, T. *et al.* Single Lgr5 stem cells build crypt-villus structures *in vitro* without a mesenchymal niche. *Nature* **459**, 262–265 (2009).
- Janda, C. Y., Waghray, D., Levin, A. M., Thomas, C. & Garcia, K. C. Structural basis of Wnt recognition by Frizzled. *Science* **337**, 59–64 (2012).
- Liu, P. *et al.* Requirement for Wnt3 in vertebrate axis formation. *Nature Genet.* **22**, 361–365 (1999).
- Yin, X. *et al.* Niche-independent high-purity cultures of Lgr5⁺ intestinal stem cells and their progeny. *Nature Methods* **11**, 106–112 (2014).
- Hao, H.-X. *et al.* ZNRF3 promotes Wnt receptor turnover in an R-spondin-sensitive manner. *Nature* **485**, 195–200 (2012).
- Koo, B.-K. *et al.* Tumour suppressor RNF43 is a stem-cell E3 ligase that induces endocytosis of Wnt receptors. *Nature* **488**, 665–669 (2012).
- Chen, P.-H., Chen, X., Lin, Z., Fang, D. & He, X. The structural basis of R-spondin recognition by LGR5 and RNF43. *Genes Dev.* **27**, 1345–1350 (2013).
- Schwank, G. *et al.* Functional repair of CFTR by CRISPR/Cas9 in intestinal stem cell organoids of cystic fibrosis patients. *Cell Stem Cell* **13**, 653–658 (2013).
- Lecourtios, M., Alexandre, C., Dubois, L. & Vincent, J.-P. Wingless capture by Frizzled and Frizzled2 in *Drosophila* embryos. *Dev. Biol.* **235**, 467–475 (2001).
- Gurney, A. *et al.* Wnt pathway inhibition via the targeting of Frizzled receptors results in decreased growth and tumorigenicity of human tumors. *Proc. Natl Acad. Sci. USA* **109**, 11717–11722 (2012).
- Chen, B. *et al.* Small molecule-mediated disruption of Wnt-dependent signaling in tissue regeneration and cancer. *Nature Chem. Biol.* **5**, 100–107 (2009).
- Ritsma, L. *et al.* Intestinal crypt homeostasis revealed at single-stem-cell level by *in vivo* live imaging. *Nature* **507**, 362–365 (2014).
- Habib, S. J. *et al.* A localized Wnt signal orients asymmetric stem cell division *in vitro*. *Science* **339**, 1445–1448 (2013).

Supplementary Information is available in the online version of the paper.

Acknowledgements We thank M. van den Born, C. Kroon-Veenboer, J. van Es, T. Darvishi and S. van den Brink and the Hubrecht imaging facility for technical support. We thank A. Gurney for the pan-Fzd antibody and B.-K. Koo for discussions. M.M.M. is supported by the European Research Council (ERC StG 242958), the European Union (FP7 Marie-Curie ITN 608180 'WntsApp') and the Netherlands Scientific Organization (NWO-ECHO 711.013.012 and NWO-VICI 91815604).

Author Contributions H.F.F. conceived the study, performed the experiments and wrote the manuscript. I.J. and O.B. performed experiments and provided intellectual input. M.H.M. and D.V.F.T. performed experiments. J.K. performed ES blastocyst injection. K.P., S.A. and P.J.P. provided microscopic support and reagents. M.M.M. and H.C. conceived the study and wrote the manuscript.

Author Information Reprints and permissions information is available at www.nature.com/reprints. The authors declare competing financial interests: details are available in the online version of the paper. Readers are welcome to comment on the online version of the paper. Correspondence and requests for materials should be addressed to H.C. (h.clevers@hubrecht.eu) or H.F.F. (farin@gsh.uni-frankfurt.de).

METHODS

Mice. For generation of the *Wnt3^{HA}* allele, a 1,044-base-pair genomic fragment covering the exon 2 of the gene using the primer pair forward 5'-TCCTTTGTCCTTTATATTGGATTC-3' and reverse 5'-AGGGAATGTCA CACATGTCTAC-3' was subcloned and the HA-tag was introduced using the following PCR primers: forward 5'-GGCACGTCGTATGGGTA CTGGGAGGCCAGAGATGTGAC-3' and reverse 5'-AGACTACGCATCTCT GCCTCTGCCTCTGCGGCTCCATC-3' (underlined residues encoding for the epitope tag). The fragment was subsequently amplified with primers flanked by LoxP and LoxM sites, and introduced in reverse orientation into the pL451 plasmid that contained a P_{gk}-neomycin-pA selection cassette flanked by Frt-sites by recombination cloning (In-Fusion HD, Clontech). The wild-type exon 2 and the 5'- and 3'-homology regions were introduced in a configuration that allowed excision of the wild-type exon 2 and inversion of the HA-tagged exon 2 after Cre-mediated recombination between the two pairs of LoxP and LoxM sites (Extended Data Fig. 1c). After sequence verification the linearized targeting vector was used for homologous recombination in embryonic stem cells that was confirmed by Southern blot analysis (Extended Data Fig. 1d). After blastocyst injection, chimaeric offspring was crossed to FLP_{er} mice³¹ to remove the neomycin expression cassette. Germline transmission was confirmed by PCR and mice were crossed to *Pgk-Cre³²* mice to induce germline recombination of the *Wnt3^{HA}* allele. The *Lgr5^{EGFP-IRES-CreERT2}* allele, the conditional *Wnt3^{fl}* allele and the transgenic *Vil-CreERT2* line have been described^{15,33,34}. Alleles were maintained on a mixed C57BL/6 background and littermate groups of mixed sexes were analysed at ages between 8 and 12 weeks. Experiments were performed according to guidelines and reviewed by the Animal Experiments Committee (DEC) of the Royal Netherlands Academy of Arts and Sciences.

Organoid culture. Mouse organoids were established and maintained as described^{16,18} from isolated crypts collected from the entire length of the small intestine. The basic culture medium (ENR) contained advanced DMEM/F12 supplemented with penicillin/streptomycin, 10 mM HEPES, 1 × Glutamax, 1 × B27 (all from Life Technologies) and 1 mM *N*-acetylcysteine (Sigma) that was supplemented with murine recombinant EGF (Peprotech), R-spondin1-CM (5% final volume if not indicated otherwise) and Noggin-CM (10% v/v). *Wnt3a*-CM was used where specified at 50% (v/v), if not indicated otherwise. A mycoplasma-free status was confirmed routinely. *Wnt3*-null cultures were obtained from *Vil-CreERT2*; *Wnt3^{fl/fl}* organoids after treatment with 0.5 μM 4-OH-tamoxifen overnight and were then maintained by addition of *Wnt3a*-CM. For constitutive lentiviral expression of mouse *Wnt3*, *Wnt3*-HA and *Wnt3*-Flag, the open reading frames were inserted 3' of a *Pgk* promoter in the lentiviral vector pLV.IRES-puro. For cell labelling *Pgk::EGFP-IRES-puro* or *Pgk::dsRED-IRES-puro* containing lentivirus was used and transduced as described³⁵. Puromycin (InvivoGen) was included in the medium (0.5–1 μg ml⁻¹) and fluorescent reporter expression was monitored and documented using an EVOS *fl* inverse fluorescence microscope (Life Technologies).

For bead neutralization experiments, the affinity matrix (anti-HA (clone 3F10)-coupled agarose beads, Roche) was washed thoroughly in medium before resuspension in Matrigel (in a ratio 1:6 (v/v)) and organoid embedding. Culture media were pre-incubated with 50 μl ml⁻¹ washed beads before addition. For cell re-association experiments, cells were collected 5 days after seeding, either in regular medium containing *Wnt*-CM or Paneth cell differentiation medium²¹ in the presence of 1 μM CHIR-99021 (Stemgent) and 15 μM DAPT (Sigma-Aldrich) in TrypLE Express (Life Technologies) and digested for 2 × 5 min at 37 °C followed by gentle mechanical dispersal. Cells were washed in cold medium containing 5% FBS and resuspended in medium containing 1,000 U ml⁻¹ DNase I (Roche) before filtration and centrifugation. The cells were then resuspended in medium containing 10% dissolved Matrigel (BD), 1 μM CHIR-99021 and 10 μM Y-27632 (Sigma-Aldrich). Eight thousand Paneth cells and/or 24,000 GFP-positive cells were co-seeded in 48-well suspension plates that had been pre-blocked with 5% FBS/PBS. After 24 h of re-association, the aggregates were collected, seeded in Matrigel and cultured in the presence of 1 μM CHIR-99021 which was withdrawn after 48 h. Organoid number was counted after 10 days and the experiment was replicated twice. For staining of re-associated organoids 25% (v/v) *Wnt*-CM was added to the normal culture medium to generate large mosaic spheroids, containing increased number of Paneth cells¹⁶. Here dsRED-labelled cells and non-labelled *Wnt3^{HA/HA}* cells were mixed in a 2:1 ratio. Blocking pan-Frizzled antibody (clone OMP-18R5 (ref. 27)) was added to the culture medium at a concentration of 50 μg ml⁻¹ in the presence of 3 μM CHIR-99021. For *Wnt3*-HA chase experiments, 2.5 μM IWP-2 (Stemgent) was added to the normal medium. Gefitinib (AstraZeneca, 1 μM), PD-0325901 (Sigma, 2 μM) and Palbociclib (PD 0332991, Sigma, 1.5 μM) were added 6 h before IWP-2-treatment to block the cell cycle. For pulse experiments, organoids were cultured in medium containing

Wnt-CM/IWP-2 for 3 days before washing and growth in normal culture medium with cell cycle inhibitors (as above). Time-lapse videos were recorded on a Leica AF7000 microscope using 30 min intervals.

CRISPR/Cas9 mutagenesis. Mutations in mouse organoids using the CRISPR/Cas9 technology were induced as described²⁵. For targeting of mouse *APC*, the reported single guide RNA (sgRNA)-5 and for *Rnf43* and *Znrf3* sgRNA-3 and sgRNA-2 were used, respectively. Correct targeting was confirmed by sequencing of *Escherichia coli*-cloned genomic PCR products (Extended Data Fig. 7). For each genotype, two independent clones were studied.

Immunostaining. Intestinal tissues were fixed 4% formaldehyde/PBS for 20 min at room temperature (22 °C) followed by embedding Tissue-Tek O.C.T. compound. Cryosections (50 μm) were incubated with Mouse Blocking Reagent (Vector Laboratories) and then with rat anti-HA monoclonal antibody (clone 3F10; Roche; 0.2 μg ml⁻¹) overnight at 4 °C, followed by incubation with unconjugated rabbit anti-rat IgG(H+L) (SouthernBiotech, 2.5 μg ml⁻¹, 1 h at room temperature) and BrightVision Poly-HRP-Anti Rabbit reagent (ImmunoLogic, 1 h at room temperature) that were both pre-blocked using normal mouse serum. For detection TSA (Life Technologies) was used according to the supplier's instructions with Alexa Fluor 488 tyramide diluted 1:100 in amplification buffer. Wheat Germ Agglutinin, Texas Red-X Conjugate (Life Technologies, 5 μg ml⁻¹) was applied for 1 h at room temperature before the slides were embedded using ProLong Gold Antifade reagent (Life Technologies).

For whole-mount stainings, organoids were collected in ice-cold medium, pelleted and resuspended in chilled Cell Recovery Solution (BD). After incubation (15 min on ice) and gentle mixing, organoids were washed in medium, pelleted, resuspended and fixed in 2% formaldehyde/PBS overnight at 4 °C. Organoids were subsequently permeabilized in PBS 0.1% Tween 20 (30 min at room temperature) before resuspension in blocking solution containing 0.2% normal donkey serum/PBS at 4 °C for 1 h. After incubation in anti-HA antibody (as above, 0.5 μg ml⁻¹, 4 °C overnight), three wash steps were performed at room temperature by addition of ice-cold PBS 0.1% Tween 20 and organoid sedimentation. For staining without permeabilization, organoids were fixed overnight in 2% formaldehyde/PBS containing 4% sucrose before washes in blocking buffer and incubation with primary antibody in the absence of detergent. Subsequent incubation steps for both protocols were rabbit anti-rat IgG(H+L) (as above) and BrightVision Poly-HRP-Anti Rabbit reagent (as above; 1:2 diluted in PBS with final 0.1% Tween 20, 0.1% Triton X-100). At this step Wheat Germ Agglutinin (as above), 4',6'-diamidino-2-phenylindole (DAPI), eFluor-660-conjugated rat anti-KI67 (eBioscience; clone SolA15; 0.4 μg ml⁻¹) and/or anti-mouse-Epcam-APC (eBioscience; clone G8.8; 0.5 μg ml⁻¹) were added, followed by washes and pre-equilibration in TSA amplification buffer (PBS pH 7.6 with 0.1 mM imidazole). Specimens were incubated for 30 min at room temperature in a 1:1,500 dilution of TSA (as above or using TSA-Cy3; PerkinElmer), followed by washes and mounting (as above). Specimens were documented on a Leica SP8 scanning confocal microscope using a ×20 objective and z-step size of 1 μm. A ×63 objective with 0.5 μm z-steps was used for Extended Data Fig. 4d, f.

Image analysis. Fiji software was used to generate z- and three-dimensional projections that were exported as video files. Channels were overlaid using Adobe Photoshop CS6. For co-localization analysis, presence of *Lgr5*-GFP, anti-HA and anti-Ki-67 staining was determined in each DAPI-positive cell on confocal z-projections of crypt hemispheres (*n* = 8 representative specimens). The *Wnt3*-HA range in mosaic organoids was determined on z-projected confocal images. For this, Epcam signals were imported into CellProfiler software³⁶ and analysed using the example pipeline 'Tissue Neighbours' that was adapted to trace all cell outlines. This mask was overlaid on dsRED and Alexa Fluor 488 signals to identify *Wnt3*-HA producing (dsRED negative) and *Wnt3*-HA receiving (dsRED positive) cells. Alexa Fluor 488 signals were thresholded to determine the cell-distance to the nearest producing cell: receiving cells were labelled positive only if a signal was found on a membrane side not in direct contact with an adjacent *Wnt*-HA producing cell. To omit cells that were engulfed by producers, receiving cells were excluded if they had four or more dsRED-negative direct neighbours. Cells were counted as 'no transfer' events only if they had direct dsRED-negative neighbour(s). The distance fractions were determined in each *n* = 10 representative mosaic organoids from experiments that were repeated three times. For surface-level measurement, *Wnt3*-HA and Epcam images were recorded using constant microscope settings. Pixel intensities (whole image) were measured using Fiji. For each specimen the *Wnt3*-HA intensity was normalized to the Epcam intensity to adjust for organoid size. Six representative crypt hemispheres were recorded per condition and the experiments were repeated three times.

Western blotting, *Wnt*-conditioned media and reporter assay. HEK293T cells were transfected with pcDNA3 expression vector that encoded the ORF of the mouse *Wnt3* complementary DNA (cDNA), which contained an HA epitope at the corresponding position (Q41) that was introduced by PCR mutagenesis with

the primers described above. Whole cell/organoid lysates were collected in $1 \times$ denaturing SDSpage Buffer, before western blot analysis using anti-HA (as above, $0.5 \mu\text{g ml}^{-1}$ in PBS containing 5% milk powder). For generation of Flag-tagged (Extended Data Fig. 2c) or HA-tagged (Extended Data Fig. 5f) mouse Wnt3a, an internal epitope was inserted at the equivalent position (Q38). A construct with HA-tagged mouse Wnt3a was used for Extended Data Fig. 5f. For production of Wnt-conditioned media, murine L-cells were transfected with Wnt3a constructs using FuGENE (Promega). Stable, clonal cell lines were established after selection using Zeocine. Media were harvested after 3–4 days of conditioning and analysed by western blotting using mouse anti-Wnt3a (a gift from R. Takada) and mouse anti-Flag M2 (Sigma) antibodies. HEK293T cells were transiently transfected with TOPFlash or FOPFlash reporter constructs and TK-Renilla as a transfection control. Cells were stimulated overnight with either control L-cell medium or Wnt3a-conditioned medium. Luciferase activity was measured using the Dual Luciferase Reporter kit (Promega) according to the manufacturer's protocol.

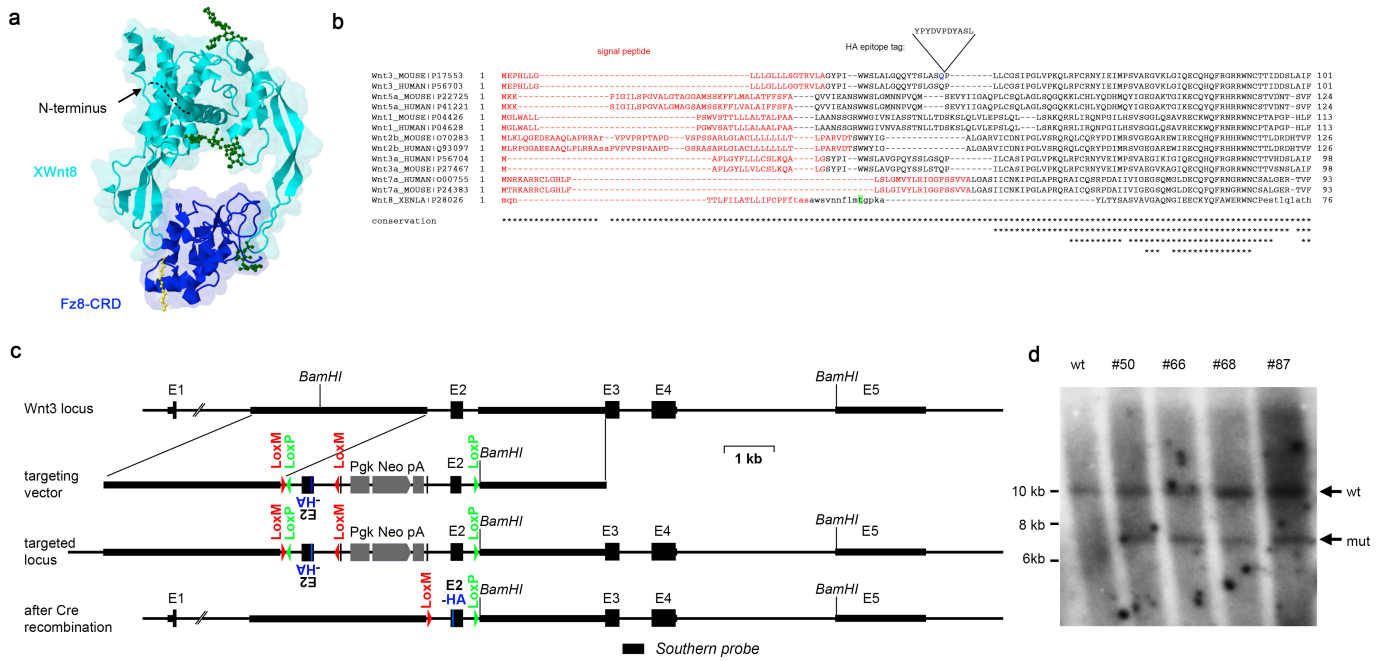
qPCR analysis. RNA preparation, cDNA preparation, qPCR and primer sequences have been described¹⁶.

EDU incorporation assay. EDU incorporation assay was performed using the Click-iT EdU Alexa Fluor 488 Flow Cytometry Assay Kit (Life Technologies). Cells were treated with $10 \mu\text{M}$ EDU 1 h before harvesting and single cell dispersal (as above) for fluorescence-activated cell sorting (FACS) analysis. Genomic DNA content was measured by addition $0.5 \mu\text{g ml}^{-1}$ 7-AAD (eBioscience) before analysis.

Statistical analysis. Sample size was chosen empirically following previous experience in the assessment of experimental variability. No statistical methods were used to predetermine sample size. Samples were not randomized and the

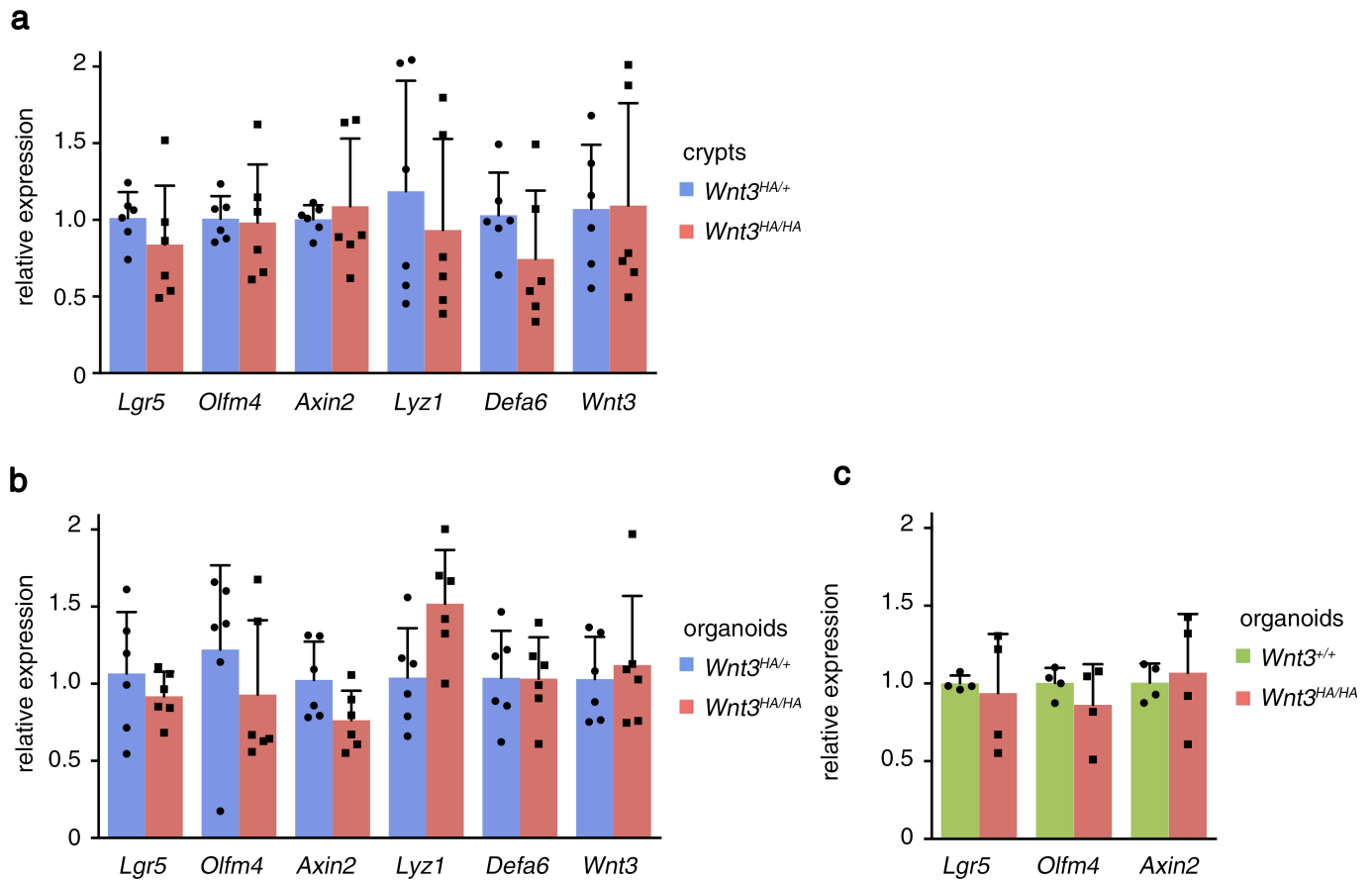
investigators were not blinded. After the normal distribution was confirmed using the Shapiro–Wilk test, significant differences between two groups were evaluated using two-tailed, unpaired Student's *t*-tests. No samples/specimens were excluded from the statistical analysis. Differences were considered to be significant when $P < 0.05$.

31. Farley, F. W., Soriano, P., Steffen, L. S. & Dymecki, S. M. Widespread recombinase expression using FLPeR (flipper) mice. *Genesis* **28**, 106–110 (2000).
32. Lallemand, Y., Luria, V., Haffner-Krausz, R. & Lonai, P. Maternally expressed PGK-Cre transgene as a tool for early and uniform activation of the Cre site-specific recombinase. *Transgenic Res.* **7**, 105–112 (1998).
33. Barrow, J. R. *et al.* Ectodermal Wnt3/ β -catenin signaling is required for the establishment and maintenance of the apical ectodermal ridge. *Genes Dev.* **17**, 394–409 (2003).
34. El Marjou, F. *et al.* Tissue-specific and inducible Cre-mediated recombination in the gut epithelium. *Genesis* **39**, 186–193 (2004).
35. Koo, B.-K. *et al.* Controlled gene expression in primary *Lgr5* organoid cultures. *Nature Methods* **9**, 81–83 (2012).
36. Lamprecht, M. R., Sabatini, D. M. & Carpenter, A. E. CellProfiler: free, versatile software for automated biological image analysis. *Biotechniques* **42**, 71–75 (2007).
37. Jmol: an open-source Java viewer for chemical structures in 3D. <http://www.jmol.org/>
38. Morgenstern, B. DIALIGN: multiple DNA and protein sequence alignment at BiBiServ. *Nucleic Acids Res.* **32**, W33–W36 (2004).
39. Schepers, A. G., Vries, R., van den Born, M., van de Wetering, M. & Clevers, H. *Lgr5* intestinal stem cells have high telomerase activity and randomly segregate their chromosomes. *EMBO J.* **30**, 1104–1109 (2011).



Extended Data Figure 1 | Generation of an epitope-tagged *Wnt3* mouse allele. **a**, Reported three-dimensional protein structure of Xwnt8 (in turquoise) bound to Fzd8-CRD (in blue) (Protein Data Bank accession number 4F0A)¹⁹. Dotted line depicts the location of the amino (N) terminus, where the HA epitope tag was introduced. Note that the position of the tag does not interfere with receptor binding. The image was created with the jmol-viewer³⁷. Glycosyl and palmitoyl groups are shown in green and yellow, respectively. **b**, Amino-acid alignment of the N-terminal region of Wnt3 and other Wnt-family members. Predicted signal peptides are indicated in red. The HA tag (YPYDVPDYASL) was inserted after position Q41 that is labelled in blue. The first residue of Xwnt8 that is resolved in the crystal structure in **a** (T32) is shaded in green. Small letters indicate non-conserved residues that could not be aligned by the software³⁸. The degree of local similarity is marked by asterisks. A score of five asterisks represents maximal similarity, which is not reached using the default settings of the algorithm. **c**, HA-knock-in strategy: a targeting

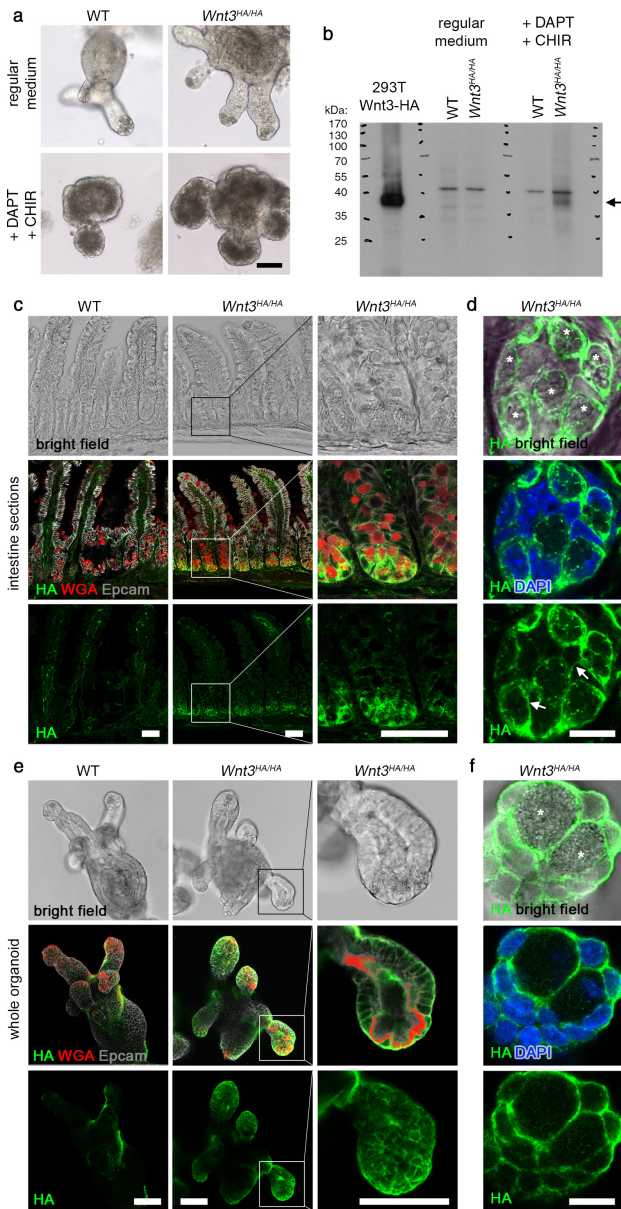
vector that comprised the normal exon 2, a Frt-site flanked P_{gk}-neomycin resistance-polyA cassette and an inverted HA-inserted exon 2 (placed in intron 1 of the gene) was used. LoxP and LoxM sites were introduced in a configuration that allowed excision of the wild-type exon 2 and inversion of the HA-tagged exon 2 by Cre-mediated recombination (orientation of LoxP and LoxM sites is indicated with arrowheads). Transgenic mice were crossed to *Pgk-Cre* mice for germline recombination of the allele. This was done because the non-recombined allele was apparently a null allele as no homozygous offspring could be obtained. We suspect that the antisense configuration of the HA-modified exon 2 could result in RNA duplex formation and masking of the regular splice acceptor site of exon 2. Consistently, we observed a shorter transcript lacking wild-type exon 2 from the non-recombined allele by RT-PCR analysis. **d**, Southern blot analysis of ES cell clones to confirm correct targeting. Genomic BamHI digest was performed (see scheme in **c**).



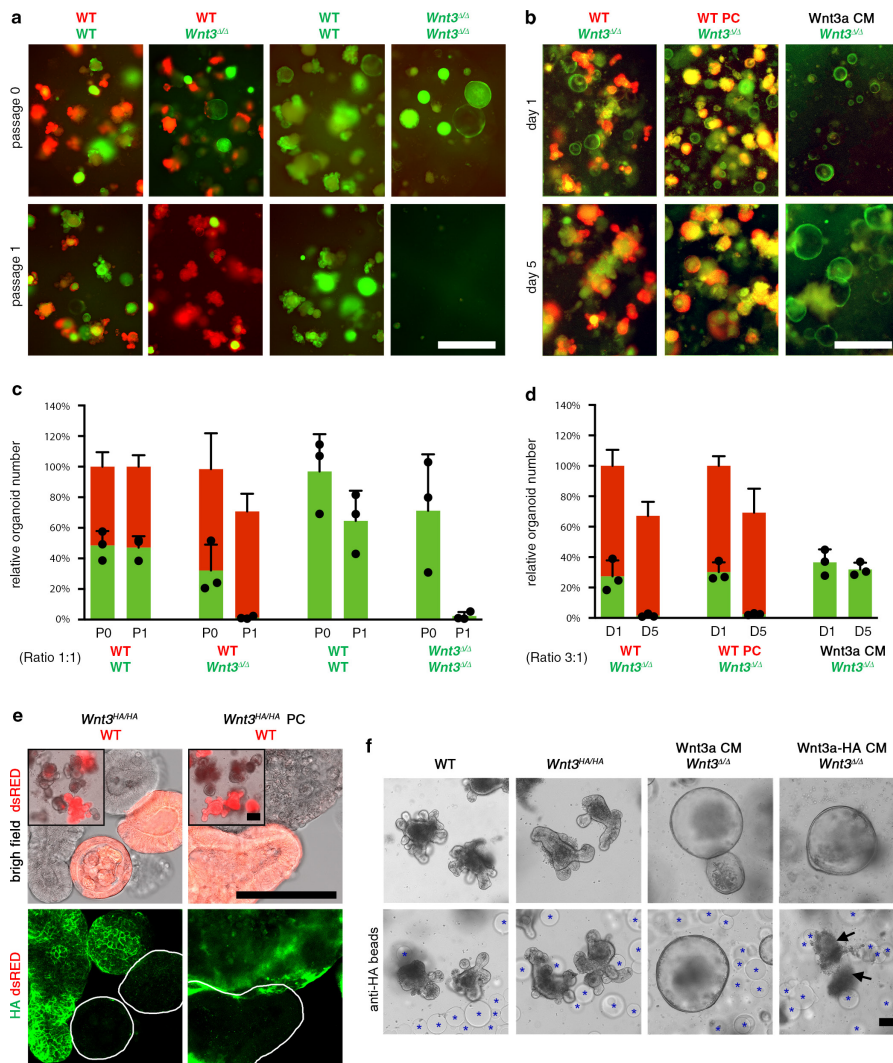
Extended Data Figure 3 | Wnt signalling status in Wnt3-HA knock-in crypts and organoids. Quantitative RT-PCR analysis of freshly isolated crypts (a) or established organoids (b, c) from the small intestine.

a, b, Mean normalized expression levels in $Wnt3^{HA/HA}$ relative to $Wnt3^{HA/+}$ -samples ($n = 6$ mice, per genotype). **c,** Relative expression

to $Wnt3^{+/+}$ organoids ($n = 4$ independent wells). Error bars, s.d., no significant changes were found ($P > 0.05$ as determined by Student's t -test). Normal expression of stem-cell markers (*Lgr5*, *Olfm4*), Wnt pathway activity (*Axin2*) and Paneth cell markers (*Lyz1*, *Defa6* and *Wnt3*) indicates that introduction of the HA-tag does not interfere with Wnt signalling.

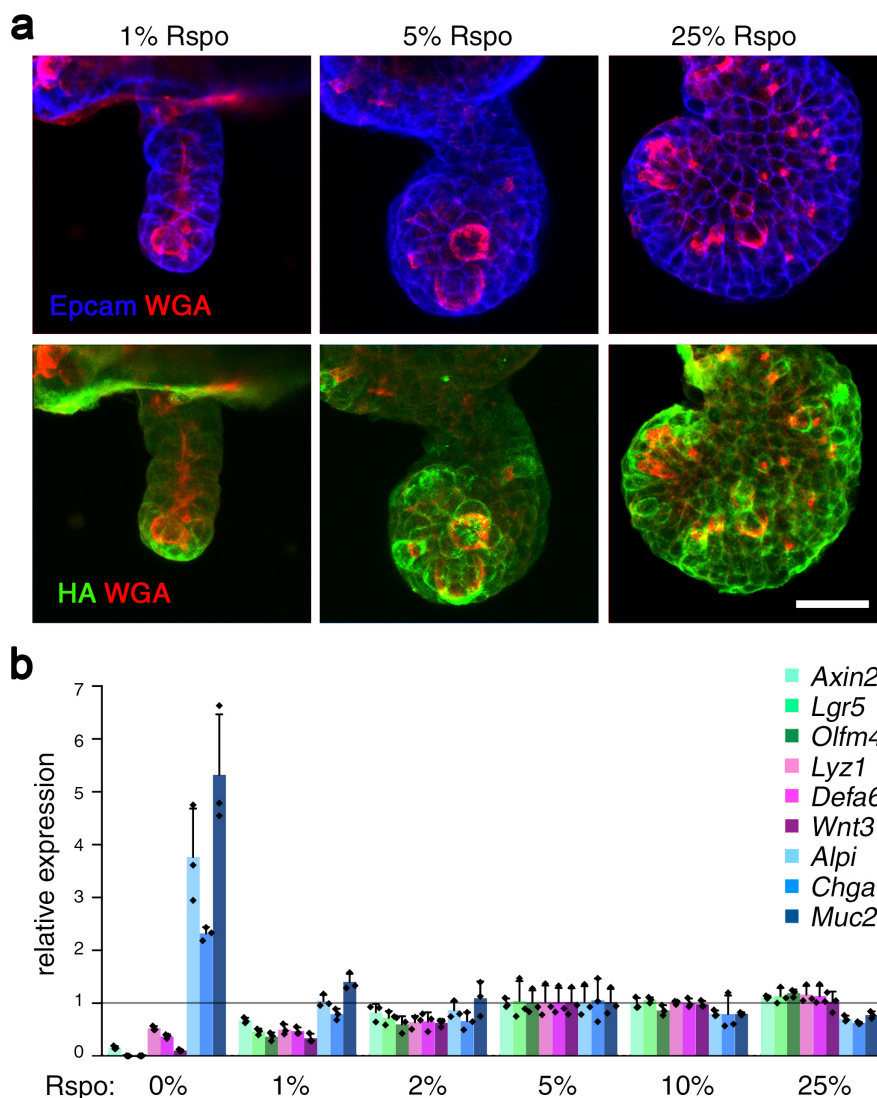


Extended Data Figure 4 | Immunodetection of endogenous Wnt3-HA protein expression. Western blot analysis using cell lysates from wild-type controls or $Wnt3^{HA/HA}$ organoids after normal culture or directed differentiation to Paneth cells (DAPT/CHIR-99021 treatment for 6 days (ref. 21)). **a**, In microscopic images, Paneth cell differentiation is evident by presence of a dark granular structure. **b**, Anti-HA western blot shows a specific signal corresponding to the Wnt3-HA protein (arrow; expected molecular mass of the mature protein chain is 39 kDa). As positive control, lysates from HEK293T cells transfected with an expression plasmid encoding the Wnt3-HA cDNA were used. Full-scan western blot is shown. **c**, Wnt3-HA staining (green signal) on small intestinal cryosections of wild-type control and $Wnt3^{HA/HA}$ mice. Counterstaining of secretory granules (wheat germ agglutinin; WGA) and cell membranes (anti-Epcam). Data from Fig. 1e are shown in bright-field and single confocal channels ($\times 20$ objective) with magnified crypt region (right). Note that the HA-signal in Paneth cells is mutually exclusive with WGA-positive apical granula. **d**, High-magnification confocal image of crypt ($\times 63$ objective) merged with bright-field channel or nuclear staining (DAPI). Paneth cells were identified by their granular morphology (asterisks); arrows label crypt membranes adjacent to Paneth cells. Single confocal image is shown (for the entire z-stack see Supplementary Video 1). **e**, Whole-mount staining of wild-type control and $Wnt3^{HA/HA}$ small intestinal organoids. Confocal images or z-projections of co-stainings as in **c** ($\times 20$ objective). **f**, High-magnification confocal image ($\times 63$ objective) of a crypt region in $Wnt3^{HA/HA}$ organoid. Scale bars, $50\mu\text{m}$ (**a**, **c**, **e**) and $10\mu\text{m}$ (**d**, **f**).



Extended Data Figure 5 | Diffusible Wnt activity in organoids is neither sufficient nor necessary to support growth. **a**, Culture after co-embedding of dsRED-labelled wild-type organoids with GFP-labelled wild-type or *Wnt3*^{Δ/Δ} organoids in Matrigel. Organoid fragments were seeded in a 1:1 ratio. *Wnt3*^{Δ/Δ} cells cannot be propagated alone or in the presence of wild-type cells. Images after seeding (P0; day 3) and after passage 1 (P1; day 10). **b**, Co-culture at higher seeding density using dsRED-labelled wild-type organoids or *in vitro* differentiated Paneth cells²¹ with GFP-labelled *Wnt3*^{Δ/Δ} organoids in a 3:1 ratio. Images of the same wells are shown at 1 and 5 days after seeding. **c**, **d**, Quantification of results shown in **a** and **b**. Mean relative number of organoids (\pm s.d.) from $n = 3$ independent experiments. **e**, Anti-HA immunodetection following

co-culture of *Wnt3*^{HA/HA} organoids or *in vitro* differentiated Paneth cells with dsRED-labelled wild-type recipient organoids (3:1 ratio). Inserts show growth in Matrigel. Confocal z-projected images are shown. Note that dsRED-positive cells remain negative for *Wnt3*-HA. **f**, Bead depletion experiment. Wild-type, *Wnt3*^{HA/HA} or *Wnt3*^{Δ/Δ} organoids were either embedded Matrigel alone or together with anti-HA affinity beads (blue asterisks) to sequester diffusible HA-tagged Wnt. Bright-field images after 6 days of culture; note that *Wnt3*^{HA/HA} organoids display unaffected morphology in the presence of beads. *Wnt3*^{Δ/Δ} organoids do not grow in the presence of beads and L-cell derived *Wnt3a*-HA CM (black arrows) demonstrating efficient depletion. Scale bars, 500 μ m (**a**, **b**) and 100 μ m (**e**, **f**).



Extended Data Figure 6 | Wnt3 protein localization and messenger RNA expression depend on the R-spondin (Rspo) concentration.
a, Wnt3-HA immunostaining (*Wnt3^{HA/HA}* organoids) after culture for 6 days in 1%, 5% or 25% Rspo-conditioned medium. Counterstaining of plasma membranes (Epcam) and secretory granules (WGA). Scale bar, 25 μ m. **b**, RT-PCR analysis of stem-cell and differentiation markers in small intestinal organoids following 6 days of culture in variable

concentrations of Rspo. Shown are mean normalized expression levels (\pm s.d.) in $n = 3$ independent wells relative to organoids cultured in the normal concentration of 5% Rspo. Markers of stem cells (*Lgr5*, *Olfm4*), Wnt activity (*Axin2*), Paneth cells (*Lyz1*, *Defa6*, *Wnt3*), enterocytes (*Alpi*), endocrine cells (*Chga*) and goblet cells (*Muc2*). Note that the messenger RNA expression of *Wnt3* is sensitive to reduced Rspo concentration.

a APC

clone#1
 WT AAAAGCGTTTTGAGTGC**CTTAT**GGAA**CCCTGTCTGCACACTGCACTGAGAATAAGGC**
 seq 5 ATGCGTTTTGAGTGCCTTAT-GAACCTGTCTGCACACTGCACTGAGAATAAGG
 seq 6 GCGTTTTGAGTGCCTTAT-GAACCTGTCTGCACACTGCACTGAGA
 seq 7 CGTTTTGAGTGCCTTAT-GAACCTGTCTGCACACTGCACTGAGAATAAGG
 seq 8 CGTTTTGAGTGCCTTAT-GAACCTGTCTGCACACTGCACTGAGAATAAGG
 seq 10 AAAAGCGTTTTGAGTGCCTTAT-GAACCTGTCTGCACACTGCACTGAGAATA

clone#2
 WT AAGCGTTTTGAGTGC**CTTAT**-GGAA**CCCTGTCTGCACACTGCACTGAGAATAA**
 seq 11 TTTGAGTGCCTTATGGGACCCTGTCTGCACACTGCACTGAGAATAAG
 seq 12 TTTGAGTGCCTTATGGGAACTGTCTGCACACTGCACTGAGAATAAGG
 seq 13 CGTTTTGAGTGCCTTATGGGAACTGTCTGCACACTGCACTGAGAATA
 seq 14 AAGCGTTTTGAGTGCCTTATGGGAACTGTCTGCACACTGCACTGAGAATAAG
 seq 15 CGTTTTGAGTGCCTTATGGGAACTGTCTGCATACTGCACTGAGAATAA
 seq 16 GCGTTTTGAGTGCCTTATGGGAACTGTCTGCACACTGCACTGAGAATAAG

b RNF43

clone#1
 WT CCGGCTGTAGACGAGCCCGAGCC--GAGTGGCCAGACTCGGGGAGTAGCTGCAGCT
 seq 9 CCCGAGCCACGAGTGGCCA
 seq 10 CCCGAGCC-CGAGTGGCCAGA
 seq 11 CCCGAGCCACGAGTGG
 seq 12 CCCGAGCC-CGAGTGGCCA
 seq 15 CCCGAGCC-CGAGTGGCCA
 seq 16 CCCGAGCCACGAGTGGCC

clone#2
 WT CCGGCTGTAGACGAGCCCGAGTGGCCAGACTCGGGGAGTAGCTGCAGCTC
 seq 17 CCCGAGC-GAGTGGCC
 seq 18 CCCGAGC-GAGTGGCC
 seq 19 CCCGAGC-GAGTGGCC
 seq 21 CCCGAGCC-AGTGGCC
 seq 22 CCCGAGCC-AGTGGCC
 seq 23 CCCGAGC-GAGTGG

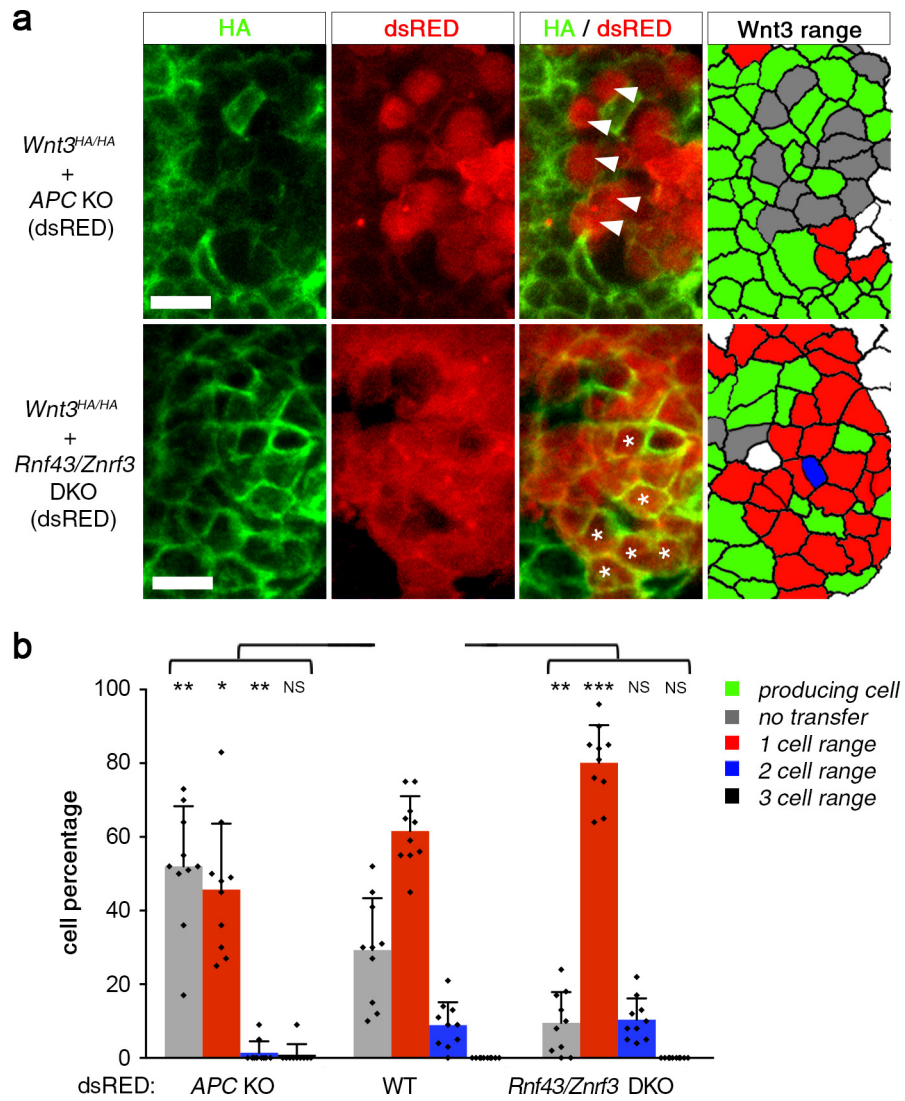
c ZNRF3

clone#1
 WT ATCCATGGCTACTGCAGCACCACAC**CTTGCCCCACTGTGCGGCACAAC**ATCATAGGTA
 seq 25 CAGCACCACACCTGCC--CACTGTCCG
 seq 26 GCAGCACCACACCTGCC--CACTGTGCGGCACAAATCATAGG
 seq 27 AGCACCACACCTGCC--CACTGTGCGGCACACATCATAGGTA
 seq 28 CAGCACCACACCTGCC--CACTGTGCGGCAAATCTAGGTAA
 seq 29 GCAGCACCACACCTGCC--CACTGTGCGGCAAATCATAGGT
 seq 30 GCAGCACCACACCTGCC--CACTGTGCGGCACAA

clone#2
 WT ATCCATGGCTACTGCAGCACCACAC**CTTGCCCCACTGTGCGGCACAAC**ATCATAGGTA
 seq 33 GCAGCACCACACCTGCC--CACTGTGCGG
 seq 34 TAGCAGCACCACACCTGCC--CACTGTGGGC
 seq 35 CAGCACCACACCTGCC--CACTGTGCGCA
 seq 36 GCACCACACCTGCC--CACTGTGCGCACA
 seq 37 CAGCACCACACCTGCC--CACTGTGCGG
 seq 38 CAGCACCACACCTG-----TCGGCACAACATCATAGGTA

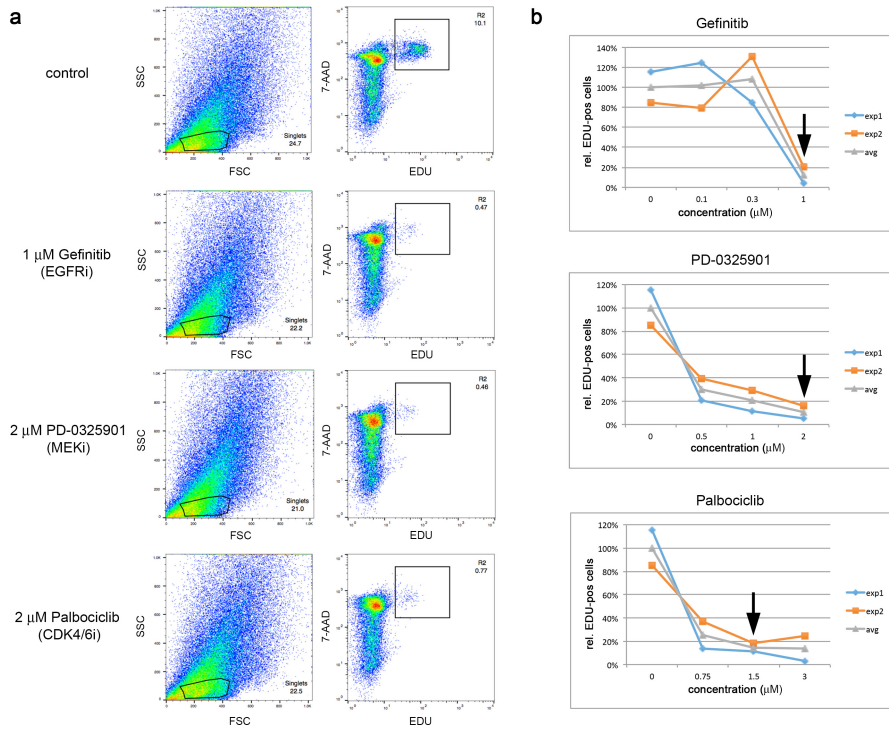
Extended Data Figure 7 | CRISPR/Cas9 induced mutations in organoids. a–c. Sequence analysis of indel mutations in targeted regions of mouse *APC* (a), *Rnf43* (b) and *Znrf3* (c) genomic loci. Two independent clonal organoid lines were analysed for each genotype. Genomic loci were PCR amplified, fragments were subcloned in *E. coli* and five or six

colonies were sequenced per clonal line. For *APC* (clone#1 and #2) and *Znrf3* (clone#1) mutant lines, hemizyosity was found, suggesting a larger genomic deletion on the other chromosome. sgRNA target sequences are shown in blue with the PAM sequence marked in bold. Arrows, Cas9 cleavage sites. Inserted nucleotides are shown in red.



Extended Data Figure 8 | Differential efficiency of Wnt3 transfer to APC- and Rnf43/Znrf3-deficient cells. a, Re-associated epithelia to test Wnt3 decoration on receiving cells (dsRED positive). The z-projected confocal images show depleted HA-signal on APC mutant cells (arrowheads) and enriched staining on Rnf43/Znrf3 mutant cells (asterisks). Wnt3 range: receiving cells were colour-coded depending on

the success of transfer and the distance to the closest Wnt3-HA neighbour. **b,** Average percentages of each distance fraction in $n = 10$ re-associated organoids (\pm s.d.). Data were compared by *t*-test to re-association experiment using wild-type receiving cells (shown in Fig. 2f). *** $P < 10^{-3}$; ** $P < 10^{-2}$; NS, non-significant. Scale bars, 10 μ m.



Extended Data Figure 9 | Pharmacological inhibition of proliferation in organoids. Cell cycle status of wild-type mouse small intestinal organoids was determined by flow cytometry. EDU incorporation assay in controls and 24 h after administration of EGFR-inhibitor (Gefinitib), MEK-inhibitor (PD-0325901) or CDK4/6-inhibitor (Palbociclib) to the regular culture medium. EDU was added 1 h before collection and dissociation of cells for FACS analysis. **a**, Original FACS data. Single cells were gated using

FSC/SSC characteristics. EDU signals were plotted against 7-AAD signals (DNA content). **b**, Inhibitor titration. Relative percentage of EDU-positive cells is shown for two independent experiments (grey line shows average). Experiments in Fig. 4 were performed at concentrations indicated by arrows. Note that Lgr5^+ intestinal stem cells double every 19–20 h *in vitro*²¹, comparable to the cell cycle length *in vivo*³⁹ (21.5 h).